# Accurate Torque Control of Finger Joints with UT Hand Exoskeleton through Bowden Cable SEA

Youngmok Yun, Priyanshu Agarwal, Jonas Fox, Kaci E. Madden, and Ashish D. Deshpande

***Abstract*— The torque control of finger joints is important for effective hand rehabilitation after neural disorders such as stroke. This paper presents an approach for accurate torque control of finger joints with UT hand exoskeleton. We present 1) how we obtained an accurate kinematics model, 2) how we built the torque actuation model with Bowden cable SEA, and 3) how we controlled the torque of finger joints with the kinematic model and the Bowden cable SEA. We have validated our approach with a testbed finger and results show that the UT hand exoskeleton accurately controls the torque of finger joints.**

## I. Introduction

Recent studies have shown that robots can help in rehabilitation process of neural disorders such as stroke [1], [2]. One major advantage of using robots for rehabilitation is high accuracy of actuation and sensing. Rehabilitation robots provide an accurate therapeutic motion based on a prescription. Rehabilitation robots measure the degree of impairments or recovery with accurate sensors, which can be reliably used in various institutions such as hospitals and insurance companies [3]. Force-controlled robots have additional advantages in rehabilitation. Force-controlled robots encourage more participation of subjects during therapy. For example, assist-as-needed (AAN) strategies prevent subjects from passively following a rehabilitation robot, and the effectiveness has been verified by clinical tests [4]. Accurately controlled force control is also advantageous for safe operation. Many subjects with neural disorders have spasticity on joints [5], which needs delicate care. Position control, without considering the stiffness of subject's joint, may cause a significant accident during rehabilitation. On the other hands, the treatment with a delicate force control can be safer.

Nevertheless, the torque control of finger joints with a hand exoskeleton is challenging. The most intuitive method is to directly match the exoskeleton joint to the finger joints and to control the exoskeleton joint torque [2], [6]. However, the design of the direct matching method is challenging particularly for multiple finger exoskeletons because of space constraints. As a result, these exoskeletons control only the grasping force of whole hand or the torque of only index finger joints. In addition, the direct joint matching design is not compatible with different hand sizes, resulting in a joint misalignment problem. To resolve these problems, hand exoskeleton developers introduced rigid-link mechanisms [7], [8] such as four-bar or glove-type mechanisms [9], [10] with cable-driven or pneumatic actuators. The introduction of mechanisms resolved the joint misalignment problem, but simultaneously brought uncertainty in the kinematics of mechanisms because finger is a part of the mechanism. The uncertainty in kinematics consequently results in uncertainty in force control of finger joints. Ueki et al. [7] estimated the overall hand length and width by using a predetermined gesture of hand poses. However, the predetermined gesture of hand poses might be challenging for subjects with neural disorders. Another technical problem is to actuate a torque in a limited space of exoskeleton. As a solution some hand exoskeleton developers adopted a remote actuation method using Bowden cable transmission [8], [11]. However, due to the substantial friction between outer sheath and inner wire, accurate force control is challenging. For lower limb exoskeletons, a series-elastic-actuator (SEA) is combined with the Bowden cable for accurate torque control [12], [13]. However, the implementation of the SEA mechanisms, which were introduced in other studies, into a hand exoskeleton is not simple mainly due to the large sizes.

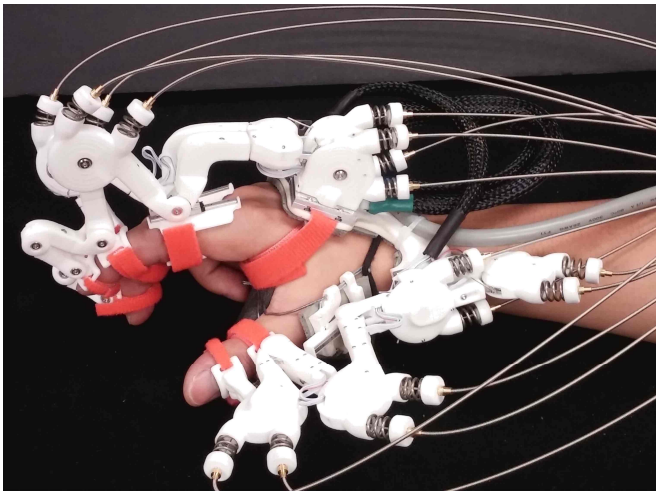

Fig. 1. UT hand exoskeleton is developed for rehabilitation and teleoperation and consists of thumb, index and middle finger modules. The exoskeleton is fabricated with Nylon-12 by a SLS machine, resulting in a light and compact design.

In this paper, we will present our approach for the torque control of finger joints with UT hand exoskeleton [14], [15], [16]. Our method includes three parts. 1) To estimate accurate joint angles of a finger, overcoming the uncertainty

Y. Yun, P. Agarwal, K. Madden are PhD students of Mechanical Engineering, The University of Texas at Austin, 3.130, ETC, Austin, Texas, USA yunyoungmok at utexas.edu

J. Fox and A. D. Deshpande are a staff and a faculty of Mechanical Engineering, The University of Texas at Austin, 3.130, ETC, Austin, Texas, USA Ashish at austin.utexas.edu

of hand sizes, 2) To model the miniature Bowden-cable SEA for torque actuation, and 3) To control the torque of finger joints with the accurate kinematics and the Bowden cable SEA. All three parts are essential for controlling the torque of finger joints with UT hand exoskeleton, but each part can be implemented for other applications because the uncertainty of hand exoskeleton kinematics and the force control with Bowden cable are common issues in robotics. In addition, we developed a testbed finger which helps in the validation of the kinematics estimation and torque actuation of finger joint. The testbed finger design and part information are shared as a supplementary material that may help other researchers' validation as well [17].

## II. UT Hand Exoskeleton

UT hand exoskeleton has been developed for rehabilitation and teleoperation. Since the first prototype of index finger exoskeleton [14], we have improved the system design and control algorithms, and recently developed an improved version of UT hand exoskeleton (Fig.1). In this paper, we will present the torque control method only for finger joints. The control of thumb joints are our ongoing work. When we developed the first prototype [14], we could not evaluate the torque control performance of the exoskeleton because the ground truth values of human finger joint were not easily accessible. While conducting pilot tests, we have found that there are several problems in the torque control of finger joints, mainly caused by the kinematics estimation and torque actuation by Bowden cable SEA. In this paper, we re-present how to control the torque of finger joints with UT hand exoskeleton, based on our previous work [14].

UT hand exoskeleton is fabricated with Nylon-12 by a selective-laser-sintering (SLS) machine for a compact design and light weight. Based on the light weight of exoskeleton (57g for finger module) and low-speed operation in rehabilitation, we assume that the inertia effect on the torque control is ignorable. That is, we assume a quasi-static condition.

We introduced four-bar mechanisms for flexion and extension of a finger. The whole four-bar mechanisms move along with the abduction/adduction of MCP, which is directly matched with the exoskeleton abduction/adduction joint (yellow in Fig. 2). The first kinematic chain (red in Fig. 2) takes advantage of a inverted-slider-crank mechanism. Due to the slider in this mechanism, the exoskeleton applies only a normal force to the proximal phalange, not causing any undesired reaction force on MCP. The second and third kinematic loops were built with basic four-bar mechanisms (blue and green respectively in Fig. 2). Since DIP joint motion is correlated with MCP and PIP [18] and the contribution of MCP abduction/adduction is small in daily activities [19], the exoskeleton does not actively actuate DIP flexion and MCP abduction/abduction. Therefore, we will control the torques of MCP and PIP joints in this paper.

UT hand exoskeleton is actuated through Bowden cable consisting of outer sheath and inner wire (commonly seen in bicycle brakes). The pulley of exoskeleton joint is connected to the pulley of motor shaft with a pull-pull mechanism

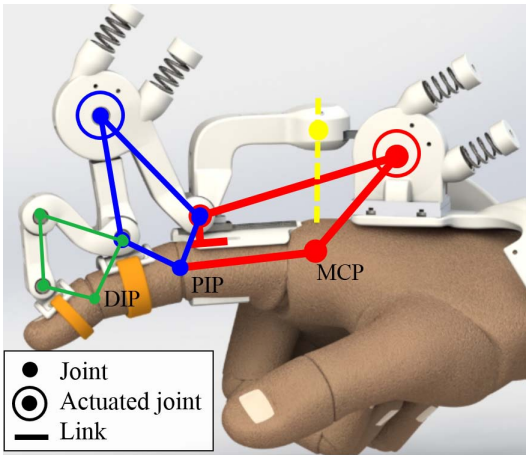


Fig. 2. The mechanism of UT hand exoskeleton. We developed a hybrid mechanism consisting of a direct matching mechanism and three four-bar mechanisms. The abduction/adduction of MCP is directly matched with exoskeleton abduction/adduction joint and flexion/extension of MCP/PIP/DIP are incorporated with four-bar mechanisms. MCP and PIP flexion are actuated through Bowden cable transmission.

(like a timing belt connection through Bowden cable. See Fig. 5). The pulley of the motor shaft is position-controlled by a servo motor system (Maxon 20 watt DC motor + 110:1 Gearhead + Maxon EPOS2 24/2). The introduction of Bowden cable as a transmission system resolved many challenges in the hand exoskeleton development. First, the Bowden cable allows for a compact design of exoskeleton. Actuating 8 DoF (2 for index finger + 2 for middle finger + 4 for thumb) in a limited space required a compact design. By locating the electric motors in a remote place, the design could be compact. Second, the Bowden cable allows for a light weight of the exoskeleton, which is important for dynamic transparency. Generally the weight of actuators such as a motor is substantial. The remote actuation reduced the weight significantly, so that we were able to ignore the inertia effect during the torque control. Third, the exoskeleton does not need to be grounded. Because the outer sheath generates a pushing force while the inner wire generates a pulling force, the sum of reaction forces in the exoskeleton is zero. Due to this unique characteristics, the exoskeleton can be easily combined with other systems such as a wrist exoskeleton [16].

## III. Accurate Kinematics Estimation with a Redundant Sensor Configuration

The introduction of four-bar mechanisms resolved the design problem and the joint alignment problem. However, the four-bar mechanisms also caused uncertainty in kinematics estimation because finger bones and joints are part of the mechanism. In this section, we will introduce how we reduced the uncertainty in kinematics estimation.

The first kinematics loop, or the inverted-slider-crank mechanism, is modeled as (1):

$$\begin{bmatrix} \theta_1 \\ x \end{bmatrix} = \begin{bmatrix} f_1(q_1, \mathbf{p}) \\ f_x(q_1, \mathbf{p}) \end{bmatrix} \tag{1}$$

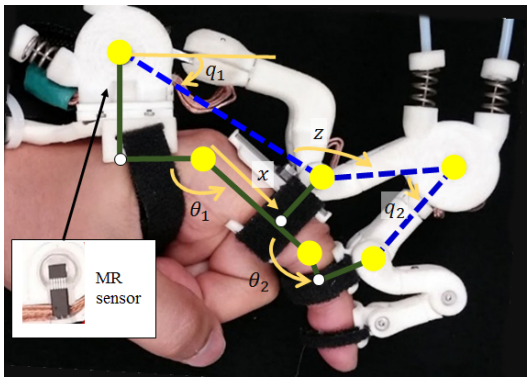


Fig. 3. The kinematics of UT hand exoskeleton. Two actively actuated joints $\mathbf{q} = [q_1 \quad q_2]^\top$ generate the MCP and PIP joint flexion of finger, denoted as $\theta = [\theta_1 \quad \theta_2]$. The kinematics equation needs link lengths of the mechanisms $\mathbf{p}$, marked in blue dotted lines and green solid lines. The exoskeleton joint angles are measured by magnetoresistive sensors and magnets that are covered by thin covers to protect them from external noise. We have introduced one extra sensor measuring the angle $z$ for the calibration of kinematic parameters of the mechanism.

where $\theta_1$ is the MCP flexion angle (Fig. 3), $x$ is the sliding length on the linear slider, $q_1$ is the first actuated joint angle of exoskeleton, and $\mathbf{p}$ is the link lengths of mechanisms and consists of $\mathbf{p}_f$ and $\mathbf{p}_e$ representing the mechanism link lengths including and excluding the kinematic parameters of finger respectively. More specifically, $\mathbf{p}_f$ and $\mathbf{p}_e$ are the lengths of the green solid lines and the blue dotted lines in Fig. 3 respectively. $\mathbf{p}_e$ is obtained from the CAD model, thus has low uncertainty. But $\mathbf{p}_f$ contains parts of finger kinematic parameters, thus has larger uncertainty than $\mathbf{p}_e$. $f_1$ and $f_x$ are determined by the equation of inverted-slider-crank mechanism. Here we omit the detailed equation due to its length. For details, see [20]. The second kinematic loop is modeled as:

$$\theta_2 = f_2(q_2, x, \mathbf{p}) \tag{2}$$

where $\theta_2$ is the PIP flexion angle, $q_2$ is the second actuated joint angle of exoskeleton, and $f_2$ is determined by the equation of four-bar mechanism [20]. $x$ is the function of $q_1$, thus one link length of the second four-bar is determined by $q_1$. As a result, $\theta_2$ is the function of both $q_1$ and $q_2$. The MCP and PIP flexion angles are rewritten as a vector form:

$$\theta = \mathbf{f}(\mathbf{q}, \mathbf{p}) \tag{3}$$

where $\theta = [\theta_1 \quad \theta_2]^\top$, $\mathbf{q} = [q_1 \quad q_2]^\top$, and $\mathbf{f} = [f_1 \quad f_2]^\top$. The major uncertainty of (3) is caused by the uncertainty of $\mathbf{p}_f$, or the kinematic parameters of finger.

Our strategy to reduce the uncertainty is to estimate the $\mathbf{p}_f$ by adding an extra sensor that measures the exoskeleton joint angle $z$ that is correlated with both the first and second kinematic loops (Fig. 3). The calibration of $\mathbf{p}_f$ is performed once after wearing the hand exoskeleton. The exoskeleton gently sweeps the RoM of finger joints. While sweeping the RoM, sensor data containing $q_1, q_2, z$ are collected. Among the collected sensor data, $N$ samples are randomly selected for optimization. Then, the $\mathbf{p}_f$ is selected by minimizing the gap between the estimated $\hat{z}$ and actual sensor values $z$:

$$\underset{\mathbf{p}_f}{\operatorname{argmin}}\, C = (\Delta\mathbf{z}^\top \Delta\mathbf{z}) \tag{4}$$

$$\Delta\mathbf{z} = \begin{bmatrix} \hat{z}_1 - z_1 \\ \vdots \\ \hat{z}_N - z_N \end{bmatrix} = \begin{bmatrix} h(\mathbf{p}_f, \mathbf{q}_1) - z_1 \\ \vdots \\ h(\mathbf{p}_f, \mathbf{q}_N) - z_N \end{bmatrix}$$

where $\mathbf{q}_i$ and $z_i$ are the sensor data of the $i$-th sample, and $h$ is the measurement model for $\hat{z}$ which is obtained by the four-bar equations. Because the measurement model is nonlinear and the number of elements in $\mathbf{p}_f$ is six, the optimization problem is not a simple convex optimization problem. However, since we are able to provide a good initial values of the optimization by measuring the link lengths with a ruler, which is close to the actual value, the optimization is normally successful. The optimization is performed by a Matlab optimization toolbox, *fmincon* with lower and upper bounds. The upper and lower bounds are determined by the level of measurement difficulty. For example, the measurement of phalange length has lower uncertainty than the measurment of the MCP location relative to the exoskeleton joint. After the calibration of $\mathbf{p}_f$ by (4), the kinematics estimator (3) seamlessly estimates the flexion angles of MCP and PIP joints.

## IV. Bowden Cable SEA Modeling and Control

The introduction of Bowden cable resolved many technical problems of UT hand exoskeleton as stated in Section II, but also introduced additional control challenges. The first problem is a low efficiency of power transmission. The friction between the inner wire and outer sheath significantly deteriorates the efficiency of power transmission. The second problem is that the friction of Bowden cable is not predictable. The friction is correlated with many factors including material property, routing path, and even time [21], [22].

Our first strategy was to find the best configuration of Bowden cable which has a high transmission efficiency and low nonlinearity. We have conducted experimental analysis with various combinations of different materials [22], and finally, we selected a steel sheath and a braided stainless steel cable. This combination provides a reasonably high efficiency due to its high stiffness, and does not have time-dependent properties. Polymer-based material such as PTFE provides a higher transmission efficiency than metal but the friction with the polymer-based material changes as operation time goes by [21]. In addition, the durability of polymer-coating is generally low, so that the coated surface on metal gets damaged during operation, deteriorating the transmission efficiency. Strong pre-tension also helped to eliminate an undesirable nonlinear effect such as slackening.

The backlash-like effect of Bowden cable has been reported by previous studies on the power transmission using Bowden cable [21], [23]. That is, the tension of inner wire in Bowden cable transmits to the other side after some displacement. The sources that cause the backlash are guessed as the elongation of inner wire due to large friction,

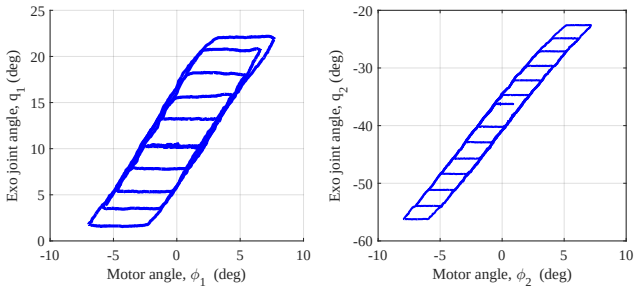


(a) Backlash at $q_1$ without disturbance

(b) Backlash at $q_2$ without disturbance

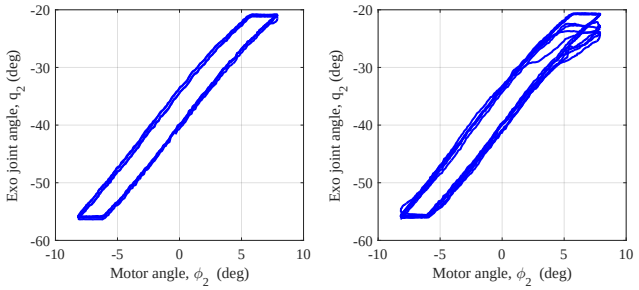


(c) Backlash at $q_2$ during a normal operation

(d) Backlash at $q_2$ with 180° cable bending

Fig. 4. Backlash effect of Bowden cable transmission. The rotational angles of exoskeleton joint pulley were measured while the pulley on the motor shaft generated a sinusoidal motion. For (a) and (b), the amplitude has been increased as time goes by. (a) shows the backlash of $q_1$ joint, (b) shows the backlash of $q_2$. (c) and (d) shows the backlash with different cable routing disturbance. (c) was measured while the routing path for the Bowden cable for $q_2$ is changed as exoskeleton operation. (d) was measured while a researcher bent the Bowden cable about 180° repeatedly.

the play between outer sheath and inner wire, motor gear head and etc. Generally, the backlash critically affects the performance of dynamic system control. However, because we assume a quasi-static condition, the torque control is still feasible with the backlash modeling. Our Bowden cables also have the backlash effect as shown in Fig. 4 (a) and (b). The exoskeleton joint angle $q_1$ and $q_2$ were measured while the corresponding motors generated sinusoidal motions without load on the exoskeleton joint. The backlash of our Bowden cable transmission is mathematically modeled as:

$$\tilde{q}(t) = BL(\phi(t))$$
$$\begin{cases} \alpha(\phi(t) - c_r), & \text{if } \dot{\phi}(t) > 0 \text{ and } \tilde{q}(t^-) = \alpha(\phi(t^-) - c_r) \\ \alpha(\phi(t) - c_l), & \text{if } \dot{\phi}(t) < 0 \text{ and } \tilde{q}(t^-) = \alpha(\phi(t^-) - c_l) \\ \tilde{q}(t^-), & \text{otherwise} \end{cases} \tag{5}$$

where $\phi$ is the pulley rotation angle on the motor shaft, $\tilde{q}$ is the modeled angle change of the pulley on the exoskeleton joint through the backlash model (5), $\alpha$ is the ratio between the pulley radius on motor shaft and the pulley radius on exoskeleton joint, or $\alpha = r_m/r_s$. $c_r$ and $c_l$ are the right and left offsets of the backlash curve, and $t^-$ indicates the time just before $t$. One notable point is that the backlash effect is correlated with the routing path of Bowden cable.

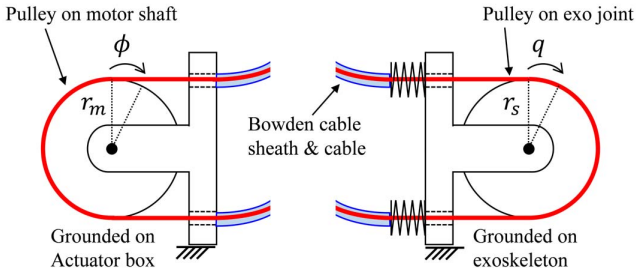


Fig. 5. UT hand exoskeleton is actuated by Bowden cable SEA. Bowden cable SEA helped the exoskeleton design to be compact and light. The SEA converts the displacement of Bowden cable into the torque on the exoskeleton joint.

The movement of joint $q_1$ causes the change of routing path of Bowden cable for $q_2$, thus we measured the backlash effect while providing different routing path disturbance for validating the consistency of the backlash model. Fig. 4 (b),(c) and (d) show the backlash at $q_2$ with and without the disturbance of routing path. Fig. 4 (b) was measured without disturbance, and the backlash effect was consistent. For Fig. 4 (c), we simulated the disturbance of routing path, that is close to a normal exoskeleton operation, about 45° bending. For Fig. 4 (d), we repeatedly bent the Bowden cable about 180° locally. The results show that we are able to use the backlash model in a normal operation, but we have to avoid a serious bending of Bowden cable for the effectiveness of the backlash model. For more quantitative analysis on the effect of cable routing, refer to our previous work [22] and [21].

The displacement of the inner wire of Bowden cable is estimated through the backlash model (5) from the motor angles, but the force control on the exoskeleton joints were still challenging because of the unpredictable friction in the Bowden cable. Hence, we introduced a Bowden-cable series-elastic-actuator (SEA) (Fig. 5). The basic principle is that two compression springs before the exoskeleton pulley convert the deflection of the compression spring into the torque. The torque of the SEA is modeled as:

$$\begin{aligned} \tau_s &= r_s(2k\Delta d) \\ &= 2kr_s^2(\tilde{q} - q) \end{aligned} \tag{6}$$

where $\tau_s$ is the torque of the SEA, $k$ is the stiffness of the compression spring, $r_s$ is the pulley radius of SEA joint, $\Delta d$ is the deflection of the compression springs representing $r_s(\tilde{q}-q)$. $q$ is the SEA angle and $\tilde{q}$ is obtained from (5). This model is assuming that the backlash model is maintained while the load of SEA changes. The model will be validated in the next section.

To control the torque of the SEA, we get the desired $\tilde{q}$, or $\tilde{q}_d$, from (6) as:

$$\tilde{q}_d = \frac{\tau_s}{2kr_s^2} + q \tag{7}$$

and we get the desired motor angle through the backlash

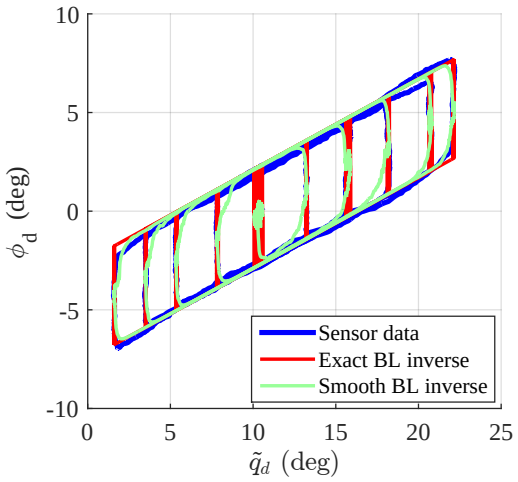


Fig. 6. The inverse of backlash model of Fig. 4 (a) for controlling the SEA torque. The exact inverse of the backlash model results in a discontinuity of the motor angle. The smoothed inverse is introduced for a smoother motor motion with a sigmoid function. (Best in color)

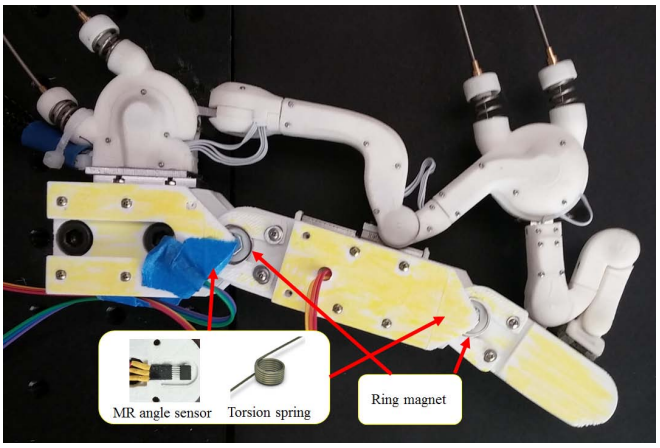


Fig. 7. A testbed finger (painted in yellow) is assembled with UT hand exoskeleton. The testbed finger is developed for the validation of a hand exoskeleton. The testbed finger contains two magnetoresistive sensors with magnet rings and two torsion springs. The angle sensors and torsion springs provide the ground-truth values of angles and torques of MCP and PIP flexion.

inverse, $BL^{-1}$, expressed as:

$$\phi_d(t) = BL^{-1}\left(\tilde{q}_d(t)\right) = \begin{cases} \tilde{q_d}/\alpha + c_l & \text{if } \dot{\tilde{q}}_d(t) > 0 \\ \tilde{q_d}/\alpha + c_r & \text{if } \dot{\tilde{q}}_d(t) < 0 \end{cases} \quad (8)$$

However, this exact backlash inverse needs a discontinuous motion of motor angle due to the discontinuity of (8), which is unrealistic and results in a jerky motion of the motor. In this regard, we implemented the smooth backlash inverse introduced in a previous study on the system control under the backlash effect [24]. The basic idea is to make a smooth transition between the two cases of (8) by using a sigmoid function. The smooth backlash inverse, $SBL^{-1}$ is expressed as:

$$\phi_d(t) = SBL^{-1}\left(\tilde{q}_d(t)\right) = \tilde{q_d}/\alpha + c_r\gamma + c_l(1-\gamma) \quad (9)$$
$$\gamma(\dot{\tilde{q}}_d(t)) = \frac{1}{1+\exp(-\rho\dot{\tilde{q}}_d(t))}$$

where $\gamma$ is the sigmoid function. $\rho$ is a positive constant, determining the degree of smoothness. As $\rho$ gets closer to zero, the sigmoid function becomes smoother. If $\rho$ is a very large value, (9) becomes same as (8). Fig. 6 shows an example of the exact backlash inverse and the smooth backlash inverse.

Finally, the torque of finger joints, MCP and PIP flexion, is controlled by the SEA torque obtained by (6) and the Jacobian derived from (3). Using the virtual work principle, the required torque of the SEAs, $\boldsymbol{\tau}_s$, is obtained as:

$$\boldsymbol{\tau}_s = \mathbf{J}^\top \boldsymbol{\tau}_f \quad (10)$$
$$\mathbf{J} = \frac{\partial \mathbf{f}}{\partial \mathbf{q}}$$

where $\boldsymbol{\tau}_f$ is the joint torque of finger joints, MCP and PIP, and $\mathbf{J}$ is the Jacobian of $\mathbf{f}$ with respect to the SEA angle vector $\mathbf{q}$.

## V. Experiment Results

In this section, we will present the experimental results for the equations that we introduced in the previous sections: 1) the kinematics of the hand exoskeleton, 2) the torque estimation and actuation of Bowden cable SEA through the backlash model, and 3) the torque control of finger joints.

We have validated the UT hand exoskeleton with a testbed finger (Fig. 7). The validation of a hand exoskeleton is tricky because the measurement of kinematic parameters are not easy even with a motion capture system due to occlusion [25] and the direct measurement of the torque of finger joints are more challenging with a human subject. In this regard, we have developed the testbed finger which contains magnetoresistive angle sensors with magnets and torsion springs on MCP and PIP flexion joints. The physical interface for a human finger was replaced for the assembly with the testbed finger. From the CAD model, we could obtain the exact kinematic parameters of the testbed finger and exoskeleton. The angle sensors and torsion springs provide the ground truth values of joint angles and torques. Because we know that the validation is challenging to all hand exoskeleton developers, we share the CAD and necessary part information online [17].

First, we validated the calibration of kinematic parameter and the estimation of joint angles. In the calibration step, the exoskeleton generated sinusoidal joint motions that sweeps full RoM, then 50 sample sensor datasets were randomly selected for calibration. We input an initial guess values of kinematic parameters then they were optimized by (4). The initial guess values were obtained by adding Gaussian random noises to the true values obtained from the CAD model, simulating the measurement noise. The standard deviations for the Gaussian noise were between 5mm $\sim$ 10mm depending on the difficulty of measurement. We repeated the optimization 100 times, and the Fig. 8 (a) shows the results that most of optimized values converged to the true

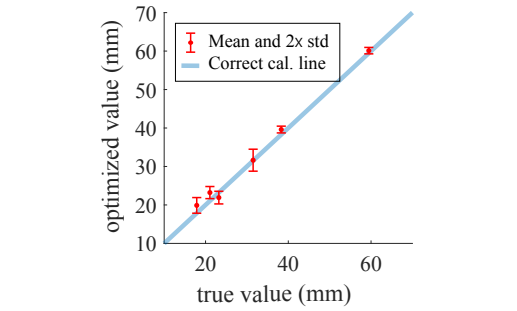


(a) Calibration result

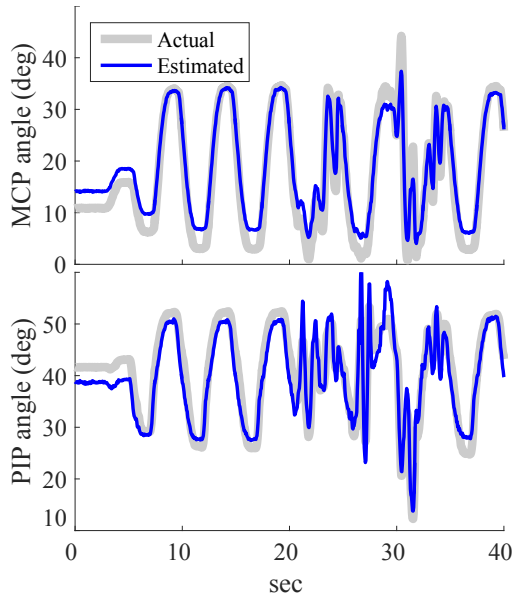


(b) Joint angle estimation

Fig. 8. Results of calibration and estimation of the exoskeleton kinematics with a testbed finger. Total six variables of $\mathbf{p}_f$ were optimized. (a) shows the distribution of optimized values after 100 iterations of optimization with random initial inputs. As the optimized values are close to the correct calibration line, the optimization is successful. (b) plots the MCP and PIP angles obtained from the testbed finger (gray lines) and estimated from exoskeleton sensors (blue lines).

values with reasonably low variance. After calibration, the joint angles of testbed finger were estimated with a calibrated kinematic parameter set selected from the 100 sets. For the first 20 seconds the SEAs moved the testbed finger, and for the next 20 seconds a researcher applied a random disturbance to simulate the torque generated by a subject. Fig. 8 (b) shows the joint angle estimation results. In the estimation, the RMS errors for MCP and PIP were 2.32 degrees and 2.86 degrees respectively. Existing estimation errors might have been caused by calibration error and sensor noise.

Next, the backlash model of (5) and the backlash inverse model (9) have been validated. For validating accurately, we attached the exoskeleton only on the proximal phalange of the testbed finger, that is, the interface for the intermediate phalange was floating during this experiment. The motor generated a sinusoidal angle (blue solid line in Fig. 9(a))

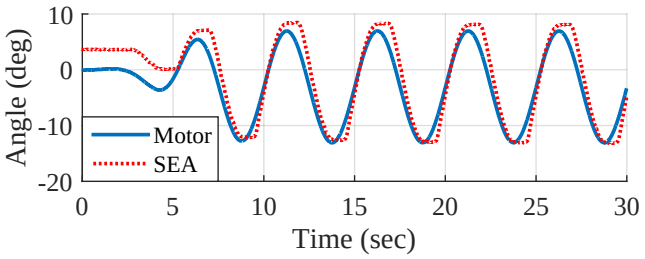


(a) Pulley angles of motor and SEA

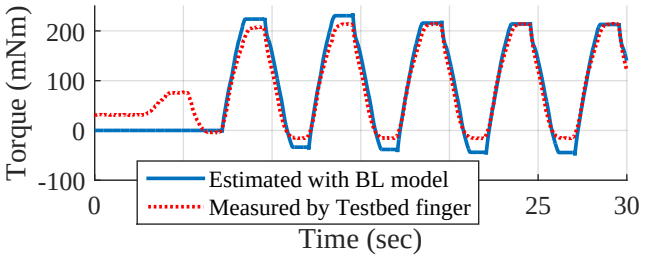


(b) Estimated and actual torque of SEA

Fig. 9. For validation of the backlash model, (5), the motor generated a sinusoidal motion and the SEA angle is measured as shown in (a). With the two curves of (a), the torque of SEA was estimated by (5) and compared with the torque derived from the testbed finger torque (b).

and we measured the SEA joint angle (red dotted line in Fig. 9(a)). With these two curves, we estimated the torque of SEA (blue solid line in Fig. 9(b)) through (5). As the ground truth (red dotted line in Fig. 9(b)), the torque measured in the testbed finger was transformed through the ratio between $q_1$ and $\theta_1$, that is $f_1$. The result shows that the backlash model is able to estimate the torque of SEA. The model was also able to estimate the dead zones that are a particular feature of backlash. To use the backlash model, the sign of velocity was required (5). However obtaining accurate velocity value from analog sensors was challenging due to noise. To avoid selecting a wrong slope of backlash model, we regarded small values of velocity as zero with a threshold. This practical approximation caused the errors in the estimation (Fig. 9(b)). Then, we validated the smooth backlash inverse model (9). The SEA generated the torque to follow a given desired torque trajectory with three different $\rho$ values which determines the smoothness of the backlash inverse model. Fig. 10 shows the result. Too high $\rho$ causes a jerky motion in torque (Fig. 10 (a)) and the motor motion (Fig. 10 (b)), and too low $\rho$ could not compensate the backlash effect. After several experiments, we select the optimum $\rho_o$ which compensates the backlash and does not make a serious jerky motion.

Finally the torque of finger joints were controlled. In the experiment, we fully connected the testbed finger with the exoskeleton. One of the calibrated parameter sets was used for the kinematics function $\mathbf{f}$ in (3). Using the $\mathbf{f}$, the Jacobian $\mathbf{J}$ was calculated, needed for (10). In the experiment, the SEAs generated torques to track desired torque trajectories. Fig. 11 shows the results of torque tracking of finger joints.

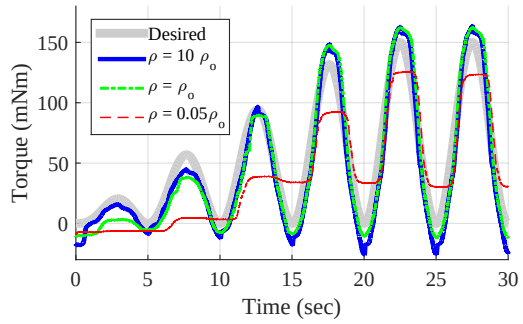


(a) Torque control of SEA

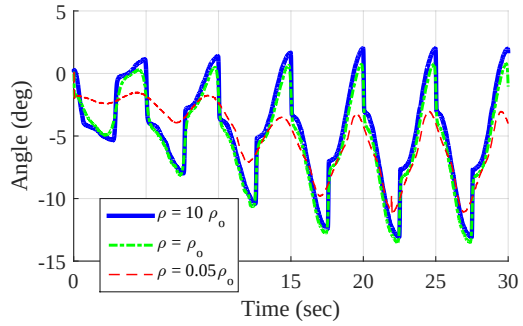


(b) Motor angle during the torque control of SEA

Fig. 10. Torque control of SEA through the smooth backlash inverse, (9). The SEA tracked the desired torque with three different $\rho$ values (a). While the SEA followed the desired torque, the motor angles were measured (b). After experiments, $\rho_o$ is selected as the optimum value of $\rho$. (Best in color)

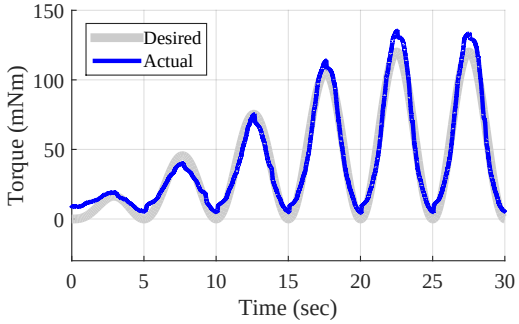


(a) Torque control of MCP joint

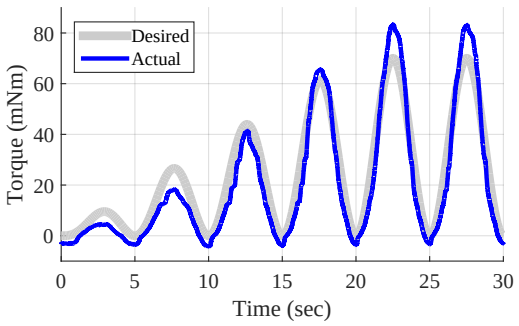


(b) Torque control of PIP joint

Fig. 11. Torque control of finger joints with UT hand exoskeleton. Using the calibrated kinematic model and the smooth backlash model, the finger joint is controlled by two SEAs. The SEAs tracked the desired torque trajectories of finger joints. The actual torques were measured from the testbed finger.

In the experiment, the RMS errors of the torque tracking for MCP and PIP were 7.66 mNm and 6.35 mNm respectively. The result reflects the effectiveness of the kinematic model, the backlash model, the smooth inverse of the backlash model and the SEA model.

## VI. Discussion

We have presented an approach to control the finger joint torques, and validated with a testbed finger. The accurate kinematic model was obtained by a redundant sensor configuration and optimization. The torque output of Bowden cable SEA was modeled by considering the backlash effect. The control of the finger joint torque was achieved by the smooth backlash inverse and by the Jacobian of the calibrated kinematic model. The results show that each of the steps work correctly, and the controlled torque values of finger joints were close to the desired values.

Even though the results showed that our approach is valid, this approach has some limitations. Firstly, the model needs several parameters which should be acquired by an operator. The backlash model needs two empirical parameters, the left and right offsets $c_l, c_r$. The parameters need to be obtained again when the routing path of Bowden cable is significantly changed. These parameters can be obtained by a sinusoidal motion of the motors as done in Fig. 4. The smoothing parameter $\rho$ also needs to be tuned by an operator to prevent a jerky motion or a too smooth backlash inverse. Generally, the highest value in the range of not causing a significant jerky motion was the best selection. Second, we have performed all validations with the testbed finger. The validation results does not ensure the same performance with a human finger. If a physical hand interface has a play between the interface and finger phalange, the kinematics model would be uncertain. Also, if an interface interferes the finger joint motion, the interference will also cause uncertainty in the torque estimation and control.

In this paper, we introduced multiple steps for the torque control of finger joints with a hand exoskeleton, but the individual steps are separately applicable to other applications. For example, the force control through a Bowden cable is challenging due to the unpredictable friction. The Bowden cable SEA configuration and modeling provide a solution for many applications which needs a remote force actuation in a limited space.

## Acknowledgment

This work was supported, in part, by the NSF Grant (No. NSF-CNS-1135949) and the NASA Grant (No. NNX12AM03G). The contents are solely the responsibility of the authors and do not necessarily represent the official views of the NSF or NASA.

## References

[1] L. Dovat, O. Lambercy, R. Gassert, T. Maeder, T. Milner, T. C. Leong, and E. Burdet, “Handcare: a cable-actuated rehabilitation system to

train hand function after stroke," *Neural Systems and Rehabilitation Engineering, IEEE Transactions on*, vol. 16, no. 6, pp. 582–591, 2008.

[2] C. N. Schabowsky, S. B. Godfrey, R. J. Holley, P. S. Lum, *et al.*, "Development and pilot testing of hexorr: hand exoskeleton rehabilitation robot," *Journal of NeuroEngineering and Rehabilitation*, vol. 7, no. 1, p. 36, 2010.

[3] G. E. Gresham, D. Alexander, D. S. Bishop, C. Giuliani, G. Goldberg, A. Holland, M. Kelly-Hayes, R. T. Linn, E. J. Roth, W. B. Stason, *et al.*, "Rehabilitation," *Stroke*, vol. 28, no. 7, pp. 1522–1526, 1997.

[4] L. L. Cai, A. J. Fong, C. K. Otoshi, Y. Liang, J. W. Burdick, R. R. Roy, and V. R. Edgerton, "Implications of assist-as-needed robotic step training after a complete spinal cord injury on intrinsic strategies of motor learning," *The Journal of neuroscience*, vol. 26, no. 41, pp. 10564–10568, 2006.

[5] C. Sköld, R. Levi, and Å. Seiger, "Spasticity after traumatic spinal cord injury: nature, severity, and location," *Archives of physical medicine and rehabilitation*, vol. 80, no. 12, pp. 1548–1557, 1999.

[6] C. L. Jones, F. Wang, R. Morrison, N. Sarkar, and D. G. Kamper, "Design and development of the cable actuated finger exoskeleton for hand rehabilitation following stroke," *IEEE/ASME Transactions on Mechatronicss*, vol. 19, no. 1, pp. 131–140, 2014.

[7] S. Ueki, H. Kawasaki, S. Ito, Y. Nishimoto, M. Abe, T. Aoki, Y. Ishigure, T. Ojika, and T. Mouri, "Development of a hand-assist robot with multi-degrees-of-freedom for rehabilitation therapy," *IEEE/ASME Transactions on Mechatronics*, vol. 17, no. 1, pp. 136–146, 2012.

[8] A. Wege and G. Hommel, "Development and control of a hand exoskeleton for rehabilitation of hand injuries," in *IEEE/RSJ International Conference on Intelligent Robots and Systems*, pp. 3046–3051, IEEE, 2005.

[9] U. Jeong, H.-K. In, and K.-J. Cho, "Implementation of various control algorithms for hand rehabilitation exercise using wearable robotic hand," *Intelligent Service Robotics*, vol. 6, no. 4, pp. 181–189, 2013.

[10] P. Polygerinos, Z. Wang, K. C. Galloway, R. J. Wood, and C. J. Walsh, "Soft robotic glove for combined assistance and at-home rehabilitation," *Robotics and Autonomous Systems*, 2014.

[11] M. Cempini, M. Cortese, and N. Vitiello, "A powered finger–thumb wearable hand exoskeleton with self-aligning joint axes," *IEEE/ASME Transactions on Mechatronics*, vol. 20, no. 2, pp. 705–716, 2015.

[12] J. F. Veneman, R. Ekkelenkamp, R. Kruidhof, F. C. van der Helm, and H. van der Kooij, "A series elastic-and bowden-cable-based actuation system for use as torque actuator in exoskeleton-type robots," *The international journal of robotics research*, vol. 25, no. 3, pp. 261–281, 2006.

[13] J. S. Sulzer, M. A. Peshkin, and J. L. Patton, "Marionet: An exotendon-driven rotary series elastic actuator for exerting joint torque," in *International Conference on Rehabilitation Robotics*, pp. 103–108, IEEE, 2005.

[14] P. Agarwal, J. Fox, Y. Yun, M. K. OMalley, and A. D. Deshpande, "An index finger exoskeleton with series elastic actuation for rehabilitation: Design, control and performance characterization," *The International Journal of Robotics Research*, vol. 34, pp. 1747–1772, Dec. 2015.

[15] K. E. Madden and A. D. Deshpande, "On integration of additive manufacturing during the design and development of a rehabilitation robot: A case study," *Journal of Mechanical Design*, vol. 137, no. 11, p. 111417, 2015.

[16] C. G. Rose, F. Sergi, Y. Yun, K. Madden, A. D. Deshpande, and M. K. O'Malley, "Characterization of a hand-wrist exoskeleton, readapt, via kinematic analysis of redundant pointing tasks," in *IEEE International Conference on Rehabilitation Robotics*, pp. 205–210, IEEE, 2015.

[17] Y. Yun, J. Fox, S. Sarkar, and A. D. Deshpande, "Testbed finger open source," `http://goo.gl/TskeMm`, 2016.

[18] J. Arbuckle and D. McGrouther, "Measurement of the arc of digital flexion and joint movement ranges," *The Journal of Hand Surgery: British & European Volume*, vol. 20, no. 6, pp. 836–840, 1995.

[19] I. M. Bullock, J. Z. Zheng, S. Rosa, C. Guertler, and A. M. Dollar, "Grasp frequency and usage in daily household and machine shop tasks," *IEEE Transactions on Haptics*, vol. 6, no. 3, pp. 296–308, 2013.

[20] R. L. Norton, "Design of machinery: an introduction to the synthesis and analysis of mechanisms and machines," 1992.

[21] V. Agrawal, *Modeling and control of cable actuated surgical robotic systems*. PhD thesis, PURDUE UNIVERSITY, 2011.

[22] D. Chen, Y. Yun, and A. D. Deshpande, "Experimental characterization of bowden cable friction," in *IEEE International Conference on Robotics and Automation*, pp. 5927–5933, IEEE, 2014.

[23] T. Do, T. Tjahjowidodo, M. Lau, T. Yamamoto, and S. Phee, "Hysteresis modeling and position control of tendon-sheath mechanism in flexible endoscopic systems," *Mechatronics*, vol. 24, no. 1, pp. 12–22, 2014.

[24] G. Tao and F. L. Lewis, *Adaptive control of nonsmooth dynamic systems*. Springer Science & Business Media, 2013.

[25] Y. Yun, P. Agarwal, and A. D. Deshpande, "Accurate, robust, and real-time pose estimation of finger," *Journal of Dynamic Systems Measurement and Control*, vol. 137, no. 3, 2015.